Astrocyte activation is suppressed in both normal and injured brain by FGF signaling

Wenfei Kang[a], Francesca Balordi[b], Nan Su[c], Lin Chen[c], Gordon Fishell[b], and Jean M. Hébert[a,1]

[a]Departments of Neuroscience and Genetics, Albert Einstein College of Medicine, Bronx, NY 10461; [b]Departments of Cell Biology and Neural Science, Smilow Neuroscience Program, New York University Langone Medical Center, New York, NY 10016; and [c]Chongqing Daping Hospital, Third Millitary Medical University, Chongqing 400042, China

Edited* by Michael V. L. Bennett, Albert Einstein College of Medicine, Bronx, NY, and approved June 16, 2014 (received for review October 30, 2013)

In the brain, astrocytes are multifunctional cells that react to insults and contain damage. However, excessive or sustained reactive astrocytes can be deleterious to functional recovery or contribute to chronic inflammation and neuronal dysfunction. Therefore, astrocyte activation in response to damage is likely to be tightly regulated. Although factors that activate astrocytes have been identified, whether factors also exist that maintain astrocytes as nonreactive or reestablish their nonreactive state after containing damage remains unclear. By using loss- and gain-of-function genetic approaches, we show that, in the unperturbed adult neocortex, FGF signaling is required in astrocytes to maintain their nonreactive state. Similarly, after injury, FGF signaling delays the response of astrocytes and accelerates their deactivation. In addition, disrupting astrocytic FGF receptors results in reduced scar size without affecting neuronal survival. Overall, this study reveals that the activation of astrocytes in the normal and injured neocortex is not only regulated by proinflammatory factors, but also by factors such as FGFs that suppress activation, providing alternative therapeutic targets.

brain damage | astrogliosis

Astrocytes are the most abundant cell type in the mammalian brain. The thin processes of protoplasmic astrocytes (gray-matter astrocytes) canvas the neural parenchyma and make contact with several other cell types. Protoplasmic astrocytes carry out a variety of functions, including maintaining the blood–brain barrier, ion homeostasis, neurotransmitter turnover, and synapse formation (1). Another major function of these astrocytes involves their activation in response to damage. Astrocyte activation, or astrogliosis, plays a central role in the response to most or all neurological insults including trauma, infections, stroke, tumorigenesis, neurodegeneration, and epilepsy. The extent of astrogliosis can influence long-term recovery, and the response of astrocytes to different insults is likely to be graded and complex (2, 3). Nevertheless, in most cases, astrocytes transiently become hypertrophic and express high levels of intermediate filaments such as GFAP, vimentin, tenascin C, and nestin, and, in cases of severe damage, astrocytes can also become proliferative and form a scar.

Astrogliosis can have beneficial and detrimental effects on recovery. Astrogliosis is essential for minimizing the spread of damage and inflammation, but it is also inhibitory for axonal and cellular regeneration. For example, in transgenic mice in which reactive astrocytes are ablated or disabled, traumatic injury leads to the lack of normal scar formation, prolonged and more widespread inflammation, and a failure to reconstruct the blood–brain barrier and maintain tissue integrity (4, 5). However, ablation or impairment of reactive astrocytes also leads to increased nerve fiber growth in the immediate vicinity of the injury site, which could improve axonal regeneration and functional recovery (4, 5). Therefore, levels of astrocyte activation are likely to be tightly regulated.

Pro- and anti-inflammatory factors operate in concert to regulate the extent of the response to damage in several organs, for example, in the skin, lungs, and joints (6, 7). In the central nervous system, factors that promote astrocyte activation have been identified, including interleukins, fibrinogen, TGF-β, NF-κB, STAT3, and others, but few factors have been identified that act directly on astrocytes to inhibit their activation (2, 3). Attenuation of Sonic Hedgehog (SHH) signaling in postnatal astrocytes leads to increased astrocytic GFAP expression in the absence of an induced injury, suggesting a role for SHH in suppressing the activation of astrocytes (8). Deletion of β-integrin in embryonic astrocytes also results in their postnatal activation, although, in this case, an indirect developmental defect could not be excluded (9). Nevertheless, the extent to which factors actively maintain astrocytes in a nonreactive state in the healthy brain or after injury to resolve their response remains unclear. Given that the multicellular response to brain injury is normally a transient process, a shifting balance between promoters and inhibitors of astrocyte activation is likely to exist during the initiation, peak, and resolution phases of the response. Even in the uninjured brain, antagonism between promoters and inhibitors of astrocyte activation might exist, with the latter prevailing.

Identifying the molecular signals that directly regulate the behavior of astrocytes in vivo has proven difficult because the response to injury involves a multitude of cell types, including astrocytes, microglia, endothelial cells, leukocytes, neurons, and others, which interact with each other depending on the stage of the response and level of damage. The approaches used to assess the function of candidate molecules in vivo have, in most cases, not specifically targeted astrocytes, making it impossible to distinguish direct from indirect effects. Therefore, much of what has been learned to date about factors that directly regulate the state of astrocytes stems from cell culture studies (2, 10).

Significance

Most if not all types of insults to the brain, including trauma, stroke, tumor growth, and neurodegeneration, for example, are believed to elicit a complex response involving several cell types. Central to this response is the activation of astrocytes. Although many proinflammatory molecules activate astrocytes, few factors are known to suppress their activation. Here we show that disrupting one particular signal specifically in adult astrocytes in the normal or injured neocortex leads to an increase in astrocyte activation. Conversely, increasing this signal after injury suppresses their activation. Therefore, at least one suppressor of astrocyte activation exists. Of potential therapeutic interest, disrupting this suppressor in astrocytes after injury results in smaller scars without affecting neuron survival.

Author contributions: W.K., G.F., and J.M.H. designed research; W.K. performed research; W.K., F.B., N.S., L.C., and G.F. contributed new reagents/analytic tools; W.K. analyzed data; and W.K. and J.M.H. wrote the paper.

The authors declare no conflict of interest.

*This Direct Submission article had a prearranged editor.

[1]To whom correspondence should be addressed. Email: jean.hebert@einstein.yu.edu.

This article contains supporting information online at www.pnas.org/lookup/suppl/doi:10.1073/pnas.1320401111/-/DCSupplemental.

A vast literature has focused on the role of FGFs in astrogliosis. FGFs have been hypothesized to promote astrogliosis based on increased immunostaining for FGF2 and FGF receptor (FGFR) 1 (FGFR1) in reactive astrocytes after injury or ischemia (e.g., refs. 11, 12) and based on increased proliferation and GFAP expression upon injections of high concentrations of FGF2 in different brain areas (e.g., refs. 13–15). However, the role FGF signaling may play in directly regulating astrocyte activation in these experiments is difficult to interpret given the high concentrations of exogenous ligand that was administered and the potential for indirect effects through other cell types affected by FGFs. Moreover, in one study, addition of FGF to cultured astrocytes decreased GFAP expression (16). Therefore, whether FGFs play a physiological role in initiating or inhibiting astrocyte activation after injury remains unknown. Here, by using gain-of-function (GOF) and loss-of-function (LOF) genetic approaches to target adult neocortical astrocytes in mice, we address the role of FGF signaling in these cells under normal conditions and after injury.

Results

FGF Signaling Is Active in Cortical Astrocytes. To manipulate gene expression in adult astrocytes, we used a *Nestin-CreER* transgenic mouse line (17) that fortuitously and efficiently recombines astrocytes. Adult mice carrying *Nestin-CreER* and a GFP reporter allele (18) were administered tamoxifen (TM) and examined 2 wk later. In the forebrain of these mice, astrocytes ($S100^+$) were recombined and expressed GFP, whereas neurons ($NeuN^+$), microglia ($Iba1^+$), or oligodendrocyte lineage cells ($Olig2^+$ or $NG2^+$) were unrecombined (GFP-negative; Fig. 1*A* and Fig. S1*A*). The stem cell niches and ependymal layer also contained recombined cells (as described later). At 7 or 120 d after inducing recombination with TM, more than 99% of GFP^+ cells in the neocortex expressed the astrocytic marker s100 and exhibited a characteristic bush-like morphology, whereas fewer than 1% of GFP^+ cells were $NeuN^+$ neurons (Fig. 1*A*). Conversely, 85 ± 3.3% of $s100^+$ cortical astrocytes expressed GFP. Virtually no GFP^+ cells were detected in the neocortex without TM treatment, confirming a strict TM dependency of the recombination (Fig. S1*B*).

FACS of GFP-positive and -negative cortical cells followed by real-time PCR further confirmed that recombined GFP^+ cells are astrocytes because they express the gene for the astrocyte marker GFAP but not the neuronal genes *Tbr1* or *Fox3* (Fig. 1*B*). GFP-negative cells, which are largely a mix of unrecombined astrocytes and neurons, express astrocytic and neuronal markers. In addition, GFP^+ astrocytes express the FGFR genes *Fgfr1*, *Fgfr2*, and *Fgfr3*, and genes whose expression is typically induced

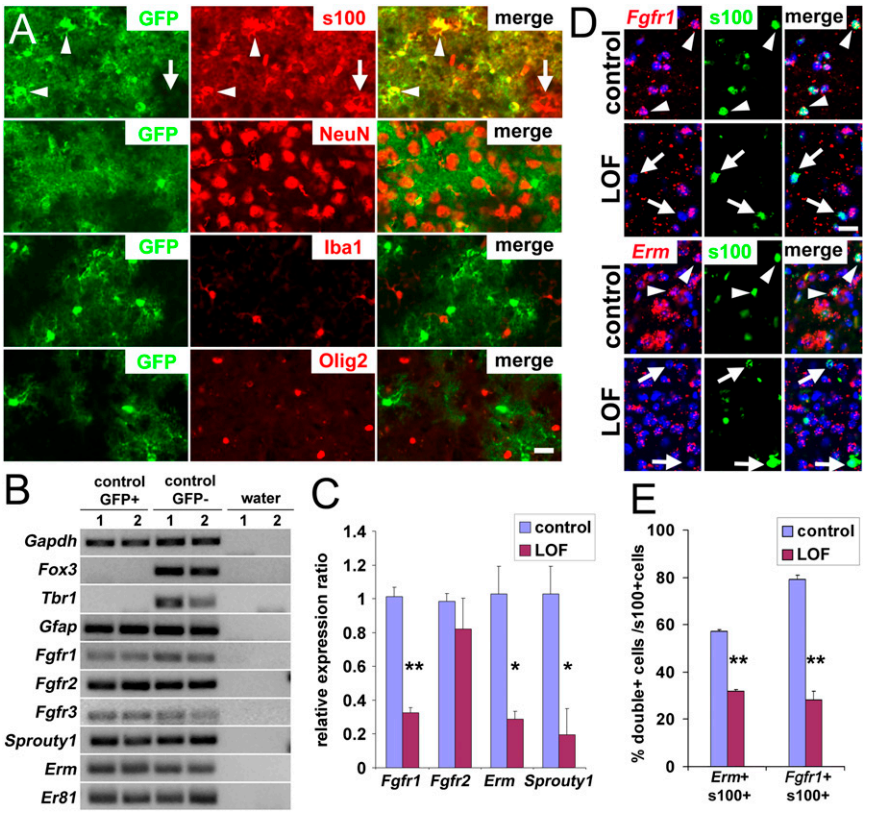

Fig. 1. Removal of FGF signaling in adult cortical astrocytes. (*A*) Sections of brains were collected and stained 2 wk after TM treatment of *Nestin-CreER* mice carrying a universal Cre-reporter allele, *Rosa26*$^{lox\text{-}stop\text{-}lox\text{-}EGFP}$. More than 99% of recombined cells (GFP^+, green) are astrocytes ($s100^+$, red) with a characteristic bush-like morphology; fewer than 1% are neurons ($NeuN^+$, red), and no recombined microglia (Iba^+, red) or $Olig2^+$ precursors (red) can be detected. Colabeling was determined by using confocal microscopy, and colabeled cells were manually counted. (*B*) FGF signaling is active in cortical astrocytes. Quantitative real-time PCR of RNA from FACS-purified GFP^+ astrocytes and GFP^- cells reveals expression of *Fgfr1*, *Fgfr2*, and FGF-responsive genes (*Sprouty1*, *Erm*, *Er81*). The neuronal markers *Fox3* and *Tbr1* confirm the purity of the astrocytes. (*C*–*E*) FGF signaling is down-regulated in the FGFR mutants 3 wk after TM treatment. (*C*) Quantitative real-time PCR analysis for FACS purified GFP^+ astrocytes from control and mutant cortices indicates a decrease in FGFR expression and signaling in the LOF mutant (mean ± SEM, $*P < 0.05$ and $**P < 0.001$). (*D* and *E*) Colabeling by in situ hybridization for *Fgfr1* or *Erm* mRNA and immunostaining for s100 reveals that fewer astrocytes express *Fgfr1* and *Erm* in the mutant cortex. A cell was considered positive for *Fgfr1* or *Erm* if more than five bright spots, a threshold set as being above background, were found in contact or overlapping with the Hoechst-stained nucleus (blue). Arrow, colabeled cells; arrowhead, astrocytes not expressing *Erm* or *Fgfr1*. (Scale bars: 20 μm.)

by FGFs, *Erm* and *Er81*, both of which are members of the Ets transcription factor gene family, and *Sprouty1*, which encodes a feedback antagonist of receptor tyrosine kinase signaling, indicating that FGF signaling is normally active in protoplasmic astrocytes (Fig. 1*B*).

Deletion of FGFRs in Cortical Astrocytes Leads to Astrogliosis. To disrupt FGF signaling in adult cortical astrocytes, *Nestin-CreER* was used to delete floxed alleles of *Fgfr1* and *Fgfr2* in an *Fgfr3*-null background. Adult *NestinCreER*;*Fgfr1*$^{fx/fx}$;*Fgfr2*$^{fx/fx}$;*Fgfr3*$^{-/-}$ animals (hereafter LOF mutants) and littermates heterozygous for all three Fgfr floxed alleles or not carrying *Nestin-CreER* (hereafter controls) were examined 2 or 4 wk after TM treatment. In FACS-purified cortical astrocytes from LOF mutants and controls that carried *Nestin-CreER* as well as the GFP reporter, mRNA levels for *Fgfr1*, *Erm*, and *Sprouty1* were decreased, as expected (Fig. 1*C*; note that, because of more variable levels of recombination for *Fgfr2*, only a trend toward decreased expression of this gene, without reaching statistical significance, was observed, but, as described later and in Table 1, recombination of *Fgfr2* is nevertheless required to obtain a strong phenotype). Colabeling with an antibody for s100 and an RNA probe for *Fgfr1* or *Erm* confirmed a decrease in FGFR expression and signaling in cortical astrocytes in mutants (Fig. 1 *D* and *E*). Interestingly, in controls, only ∼58% of astrocytes in the cortex express *Erm*, suggesting yet a new source of heterogeneity in the astrocyte population (1).

The gross morphology of the cortex and the distribution of s100$^+$ astrocytes were indistinguishable between LOF mutants and controls 14 and 60 d after TM treatment. However, some s100$^+$ astrocytes in the mutant appeared hypertrophic (Figs. 2 and 3*A*), suggesting that they might be reactive, a state normally indicative of damage. Increased GFAP expression in astrocytes is a canonical marker for astrogliosis that is especially useful in the neocortex, where expression is normally undetectable outside the corpus callosum by using standard immunohistological techniques. At both time points after TM treatment, GFAP was highly expressed in cortical astrocytes in mutants, whereas, in controls, GFAP expression was restricted to the corpus callosum (Fig. 2 *A* and *B* and Fig. S2). The presence of reactive astrocytes was confirmed by using independent markers. Vimentin and tenascin C were also up-regulated specifically in GFAP$^+$ astrocytes in the mutant but not the control neocortex (Fig. 2*B*). In addition, Nestin, which is transiently increased in reactive astrocytes (19, 20), was found to colabel a subset of GFAP$^+$ astrocytes at the 14-d time point in mutants (Fig. 2*B*). Finally, cell volume measurements using the GFP reporter allele confirmed the hypertrophic state of astrocytes with high GFAP levels (littermate controls, 3,179 ± 361 μm^3; LOF mutants, 7,966 ± 2,651 μm^3; P = 0.033; three separate experiments were performed and at least five cells were measured for each animal). Thus, LOF mutants exhibit reactive astrocytes in the cortex.

Interestingly, the deletion of FGFR genes caused the activation of astrocytes in the neocortex and hippocampus, dorsal telencephalic derivatives, but not the striatum, a ventral structure, despite efficient recombination in striatal astrocytes (compare the striatum in Figs. S1*B* and S2). This suggests that FGF signaling does not play a role in suppressing astrogliosis in ventral telencephalic regions, or, alternatively, that other signals, perhaps SHH, can compensate for the loss of FGF signaling in ventral but not dorsal regions.

Table 1. Genotypes of mice tested for the presence of astrocytic GFAP expression in the neocortex

Genotype*	No TM	With TM
Fgfr1$^{fx/?}$;*Fgfr2*$^{fx/?}$;*Fgfr3*$^{+/+}$	No	No
Fgfr1$^{fx/fx}$;*Fgfr2*$^{fx/fx}$;*Fgfr3*$^{-/-}$	No	No
Nes-CreER;*Fgfr1*$^{fx/fx}$;*Fgfr2*$^{fx/+}$;*Fgfr3*$^{+/-}$	No	No
Nes-CreER;*Fgfr1*$^{fx/+}$;*Fgfr2*$^{fx/fx}$;*Fgfr3*$^{+/-}$	No	No
Nes-CreER;*Fgfr1*$^{fx/+}$;*Fgfr2*$^{fx/fx}$;*Fgfr3*$^{-/-}$	No	+
Nes-CreER;*Fgfr1*$^{fx/fx}$;*Fgfr2*$^{fx/fx}$;*Fgfr3*$^{+/-}$	No	No
Nes-CreER;*Fgfr1*$^{fx/fx}$;*Fgfr2*$^{fx/+}$;*Fgfr3*$^{-/-}$	No	+
Nes-CreER;*Fgfr1*$^{fx/fx}$;*Fgfr2*$^{fx/fx}$;*Fgfr3*$^{-/-}$	No	+++

no, no increase in GFAP$^+$ cells; +, detectable but minor increase in GFAP+ cells; +++, large increase in GFAP$^+$ cells.
*$n \geq 3$ mice per genotype.

Loss of FGFRs in Astrocytes Induces the Activation of Microglia. To further characterize the extent of astrocyte activation, we examined other features that sometimes accompany astrogliosis such as infiltrating CD45-positive leukocytes or an increase in proliferation of oligodendrocyte progenitors, microglia, and/or astrocytes themselves (4, 21–23). No infiltrating CD45$^+$ leukocytes, which can appear after injury, could be detected in the TM-treated LOF mutants. However, within the first 3–4 wk after TM treatment, there was a transient increase in proliferating microglia (Iba1$^+$) and, to a lesser extent, Olig2$^+$ cells, but not astrocytes (s100$^+$; Fig. 3 *A* and *B*). Microglia also exhibited hypertrophy, indicative of their activation. We noticed that these activated microglia formed clusters, which may be clonal, in areas containing elevated numbers of reactive astrocytes. Astrocyte and microglia activation occur concomitantly in response to cerebral insults. Experiments aimed at activating astrocytes in vivo, whether with damage or proinflammatory factors, can also result in direct activation of microglia, masking whether activation of one cell type can induce activation of the other. Here, by genetically targeting only astrocytes, we have demonstrated that their activation can induce the proliferation and activation of microglia. It remains to be seen if the converse is also true.

Loss of FGFRs Directly Causes Astrocyte Activation. Several mechanisms could potentially lead to astrocyte activation in LOF mutants. First, a developmental defect or the contribution of defects in other cell types as a result of the *Fgfr3*-null background of the otherwise conditional mutants could perhaps cause astrogliosis. However, the *Fgfr3*$^{-/-}$ single mutant was examined with or without TM injections, and it does not exhibit increased GFAP staining in the cortex (Table 1). In addition, a triple mutant in which all three FGFRs are conditionally deleted specifically in adult astrocytes (*Nestin-CreER*;*Fgfr1*$^{fx/fx}$;*Fgfr2*$^{fx/fx}$;*Fgfr3*$^{fx/-}$) was subsequently examined and, as for the LOF mutants, it exhibits a dramatic increase in GFAP expression and cell hypertrophy (Fig. S2 *E* and *F*).

Second, the manipulation itself, TM administration, and/or CreER activity, could conceivably lead to cortical damage, resulting in activated astrocytes. However, mice carrying *Nestin-CreER* and receiving TM, which are also heterozygous for Fgfr mutant alleles, homozygous for a single Fgfr mutant, or double mutant for *Fgfr1* and *Fgfr2*, do not display signs of astrocytosis (Table 1). Meanwhile, a moderate increase in GFAP immunoreactivity is observed in the cortex of *Fgfr1*;*Fgfr3* and *Fgfr2*;*Fgfr3* double mutants and a dramatic increase is observed in the Fgfr triple mutant (Table 1, Fig. 2, and Fig. S2). These data indicate that astrocytes are activated as a result of a significant or complete loss of FGF signaling rather than the potential damage caused by expression of CreER and/or administration of TM. Consistent with this conclusion, TM administration and CreER activity are only transient. Nonetheless, astrocytes maintain high levels of GFAP for more than 60 d, a time long after any transient damage caused by the genetic technique itself would have resolved.

Third, a defect in the blood–brain barrier, of which astrocytes are an important component, could potentially promote astrogliosis

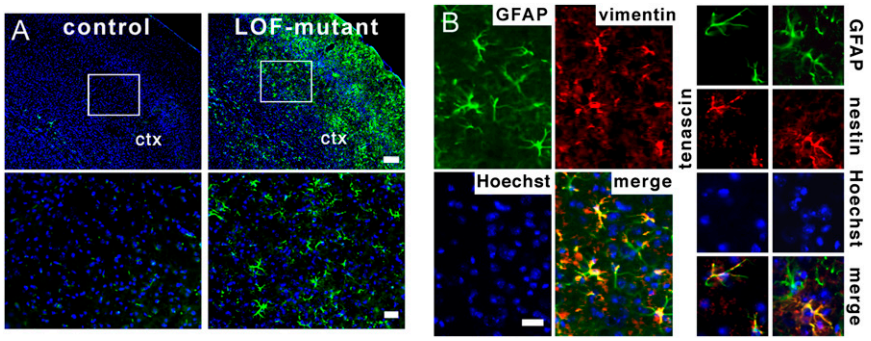

Fig. 2. Loss of FGF signaling results in the activation of astrocytes in the cortex. (*A*) The intermediate neurofilament protein GFAP (green) is increased in the neocortical gray matter (ctx) of the LOF mutant 4 wk after TM treatment. (*Lower*) Higher magnifications of boxed areas. Hoechst (blue) is used as a counterstain. (Scale bars: *Upper*, 150 μm; *Lower*, 50 μm.). (*B*) Vimentin and nestin (red) are also increased in the LOF-mutant neocortex and colabel with GFAP (green). (Scale bar: 20 μm.)

(24). Moreover, Nestin is also expressed in cells that are associated with the vasculature, albeit primarily during development (25). However, by using low- and high-molecular-weight soluble tracers in the blood (sodium fluorescein and Evans blue), no leakage into the cortical parenchyma could be detected in the LOF-mutants 3 wk after TM treatment, suggesting that the blood–brain barrier is intact (Fig. S3*A*). Moreover, laminin staining of the blood vessels also appeared intact in the mutants. Similarly, a defect in the ependymal cells, which are also targeted by *Nestin-CreER* (41.2 ± 4.9% are GFP^+ using the reporter allele), could cause at least local astrocyte activation, but the structure of the ependymal layer appears grossly normal in LOF mutants (Fig. S3 *B* and *C*).

Fourth, although cell death can trigger astrogliosis, active caspase-3 immunostaining, TUNEL assays, and Fluro-JadeB staining, which labels degenerating neurons, did not reveal any evidence of increased cell death 1, 7, 14, and 60 d after TM treatment in mutants. Conversely, even prolonged astrocyte activation did not cause neurodegeneration or cell death after 60 d (Fig. S3*D*). To formally eliminate the possibility that activation of astrocytes was induced by the less than 1% recombined neurons observed by using *Nestin-CreER*, we used *CamK2a-CreER*, which specifically targets cortical neurons, in an $Fgfr1^{fx/fx}$;$Fgfr2^{fx/fx}$;$Fgfr3^{-/-}$ background, and did not observe astrogliosis after using the same TM administration protocol and time of analysis as used with *Nestin-CreER* (Fig. 4).

Finally, although unlikely, reactive astrocytes could potentially be generated from other cells, namely precursors in the subventricular zone (SVZ) or ependymal cells, as *Nestin-CreER* in addition to recombining astrocytes also recombines SVZ cells (17) and ependymal cells (Fig. S3*B*). Moreover, severe ischemic injury immediately adjacent to the SVZ, but not superficial cortical injury, can induce the production of SVZ-derived astrocytes and their recruitment to the adjacent injury site (26). In the spinal cord, injury can induce ependymal cells to generate astrocytes (27–29). However, in the Fgfr LOF mutants, astrocytes become reactive throughout the cortex in the absence of detectable injury and in a time frame incompatible with astrocyte migration from the SVZ to all cortical areas. Nevertheless, to exclude the possibility that SVZ precursors or ependymal cells generate new astrocytes in the LOF mutants, BrdU was administered three times per day for 3 d, starting the last day of TM injections, and mice were examined 30 d later. No $GFAP^+$ astrocytes were found to colabel with BrdU in the LOF-mutant neocortex (Fig. S4*A*). This suggests that the reactive astrocytes do not derive from precursors in the SVZ, ependymal cells, or other cell types.

Although we have ruled out the more obvious potential indirect effects of a loss of FGF signaling on astrocyte activation, it remains possible that astrocytes lacking FGF signaling are dysfunctional, triggering changes in neighboring cell types that in turn activate astrocytes nonautonomously. If this is the case, not only would astrocytes that have lost FGF signaling become reactive, but those in the vicinity that retain signaling would as well. To address this possibility, we performed combined FISH and immunohistochemistry by using an anti-GFAP antibody and an RNA probe for *Fgfr1* or *Erm* transcripts. Although ∼30% of astrocytes still maintained FGF signaling in the LOF mutant (Fig. 1*E*), colabeling revealed that none of the $GFAP^+$ astrocytes in the neocortex expressed *Fgfr1* or *Erm* (Fig. 5; zero $Fgfr1^+$ or Erm^+ cells among 100 $GFAP^+$ cells), suggesting that loss of FGF signaling in a cortical astrocyte directly leads to its activation.

An investigation of the potential mechanism by which loss of FGF signaling might activate astrocytes suggested that this process was independent of the levels of candidate factors previously implicated in FGF signaling or astrocyte activation. Western blot analysis of whole cortices, despite showing an increase in GFAP expression in LOF mutants, did not reveal changes in levels of pERK (30), pAKT (30), NF-κB (3), Cdc42 (31), Lhx2 (32), and pSMAD3 (16) (Fig. S4*B*). Astrocyte activation in LOF mutants was also unresponsive to ibuprofen, a nonsteroidal anti-inflammatory agent, or rapamycin, an mTOR inhibitor and immunosuppressant (Fig. S4*C*). Nevertheless, together, the data indicate that FGF signaling is essential for maintaining cortical astrocytes in a nonreactive state in the uninjured brain.

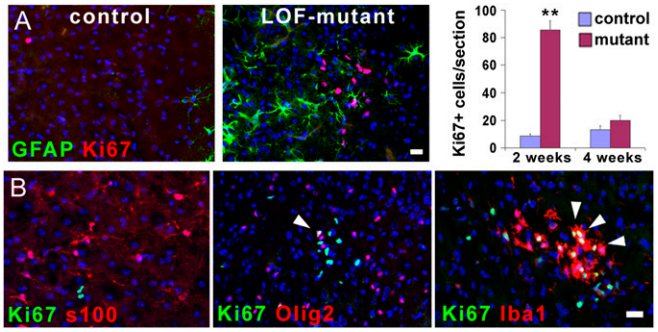

Fig. 3. Loss of FGF signaling in astrocytes induces microglia activation. (*A*) Cell proliferation, determined by immunostaining for the cell proliferation marker Ki-67 (red), is increased at 2 wk after TM treatment in the neocortex of the mutant, but then resolves back to control levels at 4 wk after TM treatment (mean ± SEM, $^{**}P < 0.001$). $Ki\text{-}67^+$ cells do not colabel with GFAP in the mutant neocortex. (*B*) The proliferating cells in the mutant are not astrocytes ($s100^+$, red), but are oligodendrocyte precursors ($Olig2^+$, red) or microglia ($Iba1^+$, red); colabeling is yellow (arrowheads). (Scale bars: 20 μm.)

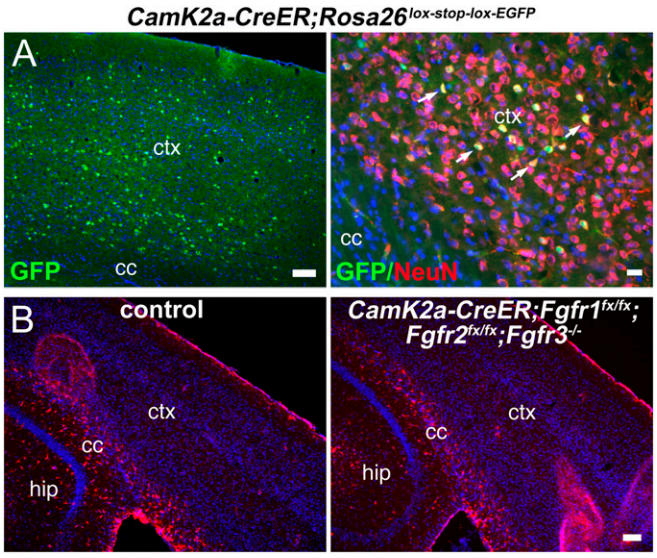

Fig. 4. Loss of FGF signaling in cortical pyramidal neurons does not induce astrocyte activation. (*A*) *CamK2a-CreER* confers recombination of a universal *Rosa26*$^{lox\text{-}stop\text{-}lox\text{-}EGFP}$ Cre-reporter allele in pyramidal neurons in the cortex. GFP$^+$ cells colabel with the neuronal marker NeuN (arrows) in the neocortex of the *CamK2a-CreER;Rosa26*$^{lox\text{-}stop\text{-}lox\text{-}EGFP}$ mice 3 wk after TM treatment. (Scale bars: *Left*, 100 μm; *Right*, 20 μm.) (*B*) No GFAP$^+$ reactive astrocytes (red) are detected in the gray matter of *CamK2a-CreER* Fgfr triple mutants 3 wk after TM treatment. cc, corpus callosum; ctx, neocortex; hip, hippocampus. (Scale bar: 100 μm.)

FGF Signaling Inhibits Astrocyte Activation After Traumatic Cortical Injury. To test how FGF signaling regulates the astrocytic response to damage, a stab wound injury was stereotaxically delivered to the neocortex (*Materials and Methods*) of LOF mutant mice and mice that conditionally express a constitutively active FGFR (i.e., GOF mutants). GOF mutant mice were generated by introducing an *Fgfr3*^{K650E} allele (33, 34) tagged to an *ires*GFP downstream of a *lox-stop-lox* cassette and a *CAG* promoter (Fig. S5*A*), and crossing the resulting transgenic line to *Nestin-CreER* mice to activate FGF signaling specifically in adult astrocytes upon TM treatment (Fig. S5*B*). In the LOF mutants, an increase in GFAP$^+$ vimentin$^+$ astrocytes was readily observed around the lesion sites as early as 24 h after injury (Fig. 6 and Fig. S5*C*), whereas, in controls and GOF mutants, astrogliosis was detected in only the white matter at this time (Fig. 6). Importantly, in the LOF mutants, the density of reactive astrocytes around the injury site was clearly higher than that in the surrounding nonlesioned areas or contralateral side, indicating that the increase in astrogliosis was an earlier or more robust response to injury compared with controls. Colabeling of S100 with GFAP indicated that the number of astrocytes (S100$^+$) had not increased, but that the proportion of astrocytes expressing elevated GFAP (S100$^+$ GFAP$^+$) had increased in the LOF mutants (Fig. S6*A*).

Consistent with an early response, at the peak stage of activation (3 d after injury), the levels of GFAP and vimentin staining around the lesion approached similar levels in controls compared with LOF mutants, whereas GOF mutants exhibited significantly less GFAP staining (Fig. 6 and Fig. S5*C*). Nevertheless, in each genotype, astrocytes were similarly hypertrophic (astrocyte size by GFAP staining, control, 478.2 ± 33.3 μm^3; LOF mutant, 456.7 ± 25.7; GOF mutant, 481.1 ± 51.3). The proliferative state of Iba1$^+$ microglia and NG2$^+$ or Olig2$^+$ oligodendrocyte precursors was also similar in all genotypes (Fig. S6*B*).

At 20 d after injury in controls, reactive astrocytes surrounding the scar tissue had mostly resolved (GFAP-negative). However, a high level of reactive astrocytes remained in LOF mutants compared with the contralateral uninjured side or the injured area of the control (Fig. 6), whereas the GOF mutants exhibited even fewer reactive astrocytes outside the lesion (in an area 130 μm from the edge of the lesion to avoid the scar tissue, see also *Cell Counts* and *Quantification of GFAP Staining Intensities After Injury* in the *Materials and Methods*). To corroborate these findings, WT adult mice received intracortical injections of lentivirus (LV) expressing constitutively active FGFR3^{K650E}-IRES-GFP (LV-FGFR3*-GFP) or GFP alone (LV-GFP). Two weeks post injection, cortex infected with LV-FGFR3*-GFP displayed a significantly lower level of GFAP staining intensity in infected (i.e., GFP$^+$) astrocytes compared with control cortices infected with LV-GFP virus (Fig. S5 *D* and *E*). Together, these data indicate that signaling through FGFRs in astrocytes is normally inhibitory to their reactive state after injury and delays initiation of gliosis and accelerates its resolution.

In the spinal cord, ependymal cells express the proliferation marker Ki-67 and act as stem cells after injury to produce astrocytes (27–29). Although previous evidence indicates that ependymal cells cannot act as stem cells in the forebrain (35–37), we nevertheless addressed the possibility that ependymal cells might be generating astrocytes in the neocortex of Fgfr LOF mutants after injury. For ependymal cells to be generating the large numbers of reactive astrocytes found throughout wide neocortical areas of the LOF mutants after injury, ependymal cells would need to proliferate asymmetrically in response to injury, producing astrocytic cells and new ependymal cells. Of note, transdifferentiation of ependymal cells to astrocytes without proliferation can be excluded given that there is no significant loss of ependymal cells in the mutants (Fig. S3 *B* and *C*). If ependymal cell proliferation were induced, these cells would express Ki-67$^+$. However, unlike in the spinal cord, ependymal cells surrounding the lateral ventricles, including the sites closest to the injury, do not express Ki-67 at 1 or 3 days postinjury (dpi) (Fig. S7). Therefore, ependymal cells in the forebrain are not likely to be producing astrocytes after injury.

Disrupting FGF Signaling Reduces Scar Size. Severe brain injuries are accompanied by scar formation, whereby astrocytes form a dense overlapping network of processes at the edges of the lesion. Although scars are complex and include components other than overlapping reactive astrocytes (such as microglia, endothelial cells, and ECM), we used the intensity and density of GFAP staining as a proxy for scar size (*Materials and Methods*). At 20 d after injury, a compact glial scar around the injury site was observed in control animals (Fig. 7*A*). GOF mutants displayed thinner and less compact scars compared with controls, consistent with the inhibition of astrocyte activation. Unexpectedly,

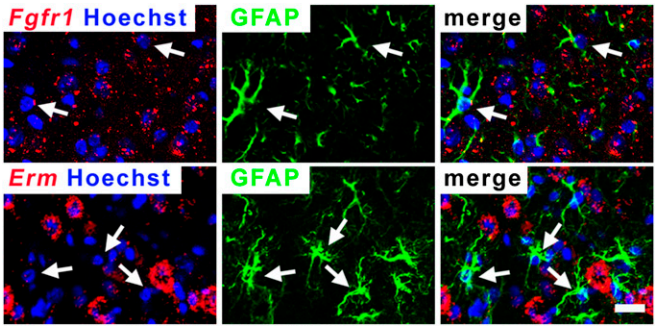

Fig. 5. Astrocytes that lack FGF signaling become reactive. Colabeling by immunofluorescence for GFAP$^+$ protein and in situ hybridization for *Fgfr1* or *Erm* RNA reveals that reactive astrocytes do not express *Fgfr1* or *Erm* mRNA in the LOF mutant (n = 0 of 100 cells examined by confocal imaging). (Scale bar: 20 μm.)

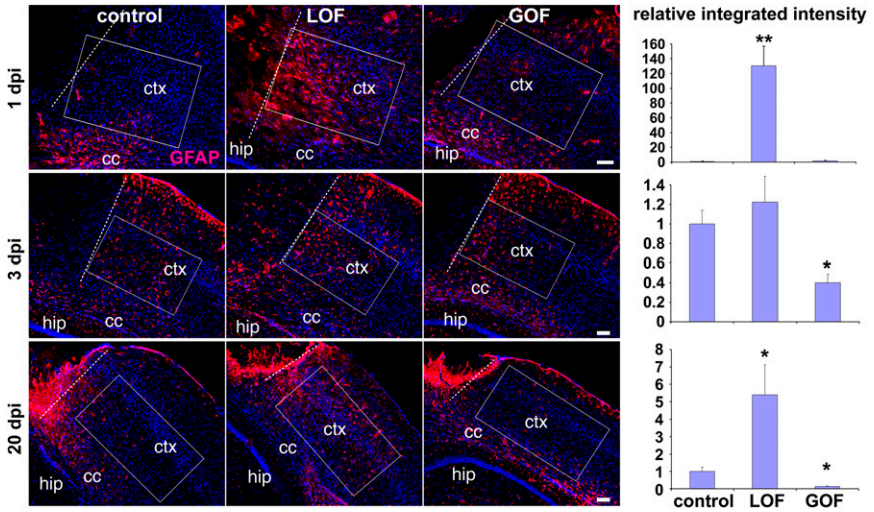

Fig. 6. FGF signaling inhibits injury-induced astrocyte activation. Controls, LOF mutants, and GOF mutants were subjected to a cortical stab wound injury 3 wk after TM treatment. Representative images of coronal sections of GFAP immunostaining (red; Hoechst, blue) were taken at 1, 3, and 20 d post injury (dpi). Integrated intensity of GFAP staining was quantified in boxed areas parallel to the plane of the neocortex (ctx) immediately adjacent to the edge of the lesion (dotted line) for 1 and 3 d post injury, 130 μm from the lesion for 20 d post injury (to avoid the scar), and, in all cases, 100 μm from the corpus callosum (cc). Intensities were normalized to the measurement in the matching position of the contralateral hemisphere. The graphs represent the relative change of the integrated intensity to the mean measurement in controls, which was set as 1 (mean ± SEM; $*P < 0.05$ and $**P < 0.001$). hip, hippocampus. (Scale bars: 100 μm.)

LOF mutants, despite persistent high levels of reactive astrocytes outside the scar tissue, also displayed thinner and less compact scars compared with controls (Fig. 7*A*). Scar formation and scar size are regulated not only by astrocyte activation, but also by astrocyte proliferation (2, 3, 10, 38). Three days after injury, the fraction of reactive astrocytes that were proliferating (Ki-67$^+$/GFAP$^+$) around the injury site was much lower in LOF mutants and greater in GOF mutants compared with controls (Fig. 7*B*), suggesting that, even though FGF signaling inhibits the activation of astrocytes, it promotes their proliferation. These dual effects on astrocytes after injury likely account for the smaller scar size upon decreased or increased FGF signaling: in LOF mutants, although there are more reactive astrocytes, their lack of proliferation reduces scar size, whereas, in GOF mutants, although astrocyte proliferation is increased, there is an insufficient number of reactive astrocytes to begin with, also resulting in a smaller scar.

Despite the differences in the number of reactive astrocytes, their proliferative state, and the size of the scar, the number of infiltrating CD45-positive leukocytes was similar in controls and

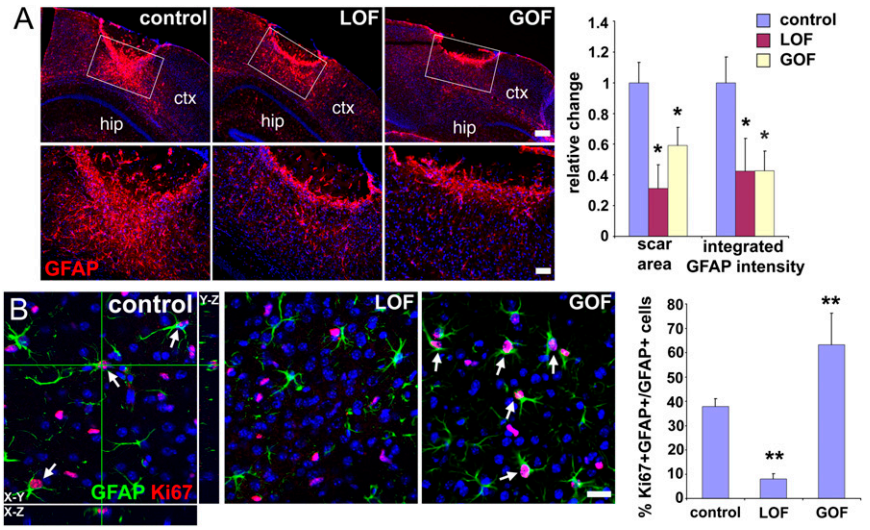

Fig. 7. Aberrant FGF signaling reduces glial scar formation. (*A*) Immunostaining for GFAP in the neocortex (ctx) 20 d after a stab wound injury reveals significantly smaller scars not only in the GOF mutants, as expected, but also, surprisingly, in the LOF mutants. The area covered by scars and the integrated intensity of GFAP staining in the scar were measured in the boxed areas as described in *Materials and Methods*. For analysis, coronal sections were positionally matched between brains along the stab wound, which extends perpendicularly to the section along the anterior–posterior axis and which, because of the triangular shape of the blade, is deeper in more posterior areas. Changes are relative to the mean value obtained for controls (set as 1; mean ± SEM; $*P < 0.05$). hip, hippocampus. (Scale bars: *Upper*, 200 μm; *Lower*, 50 μm.) (*B*) Proliferation (Ki-67 staining) of reactive astrocytes (GFAP staining) around the lesion 3 d after injury is reduced in LOF mutants, but increased in GOF mutants, providing a potential explanation for why both mutants exhibit smaller scars. Colabeling for GFAP and Ki-67 (arrows) was quantified by confocal microscopy of 20-μm sections (mean ± SEM; $**P < 0.001$). (Scale bar: 25 μm.)

LOF mutants (Fig. S8*A*). Moreover, we could detect no change in neuronal degeneration around the injury site (Fig. S8*B*). These data suggest that the loss of FGFRs in astrocytes does not limit their ability to contain the spread of inflammation and neuronal loss.

Discussion

Despite the ubiquitous presence and functional importance of reactive astrocytes in pathological conditions of the CNS, the mechanisms regulating the initiation, extent, and resolution of astrogliosis have remained largely unclear. Progress has been difficult in part because of the complexity of the problem: several cell types, including astrocytes, microglia, endothelial cells, leukocytes, neurons, and others, are likely to interact in regulating different stages of the response to damage. The nature of the experimental approaches previously used to study the damage response in vivo, which, in most cases, have not been manipulations that target a specific cell type but affect the response as a whole, have made it difficult to tease apart functionally relevant cell–cell interactions. A good example of this is the infusion of FGF2 into the sites of injury, which led to the hypothesis that FGFs promote astrogliosis (13–15). Here, by specifically targeting astrocytes in the adult, we demonstrate that the FGF pathway directly inhibits the activation of protoplasmic astrocytes in the normal brain and after traumatic injury. We also show that, although FGF signaling inhibits astrocyte activation, it promotes their proliferation. Moreover, we show that astrocytes reactive as a result of loss of FGF signaling can activate microglia in the absence of injury, providing direct evidence for a causative interplay in the activation of these cell types. What remains unaddressed by our study is whether loss of FGF signaling in other cell types could also, under some circumstances, contribute to a reactive response.

The function of FGFs cannot be inferred from changes in expression of FGF ligands or receptors, such as the increases detected in astrocytes after injury (11, 12). Increased FGF expression and signaling could act to promote astrocyte activation, as previously suggested (11, 12), or suppress it, for example, to keep the amplitude and duration of the injury response in check by countering the large numbers of proinflammatory factors. In addition, in vivo administration of FGFs after injury can potentially affect multiple cell types so that any observed response from astrocytes can be indirectly caused by changes in other cell types. The concentrations of FGFs administered may also not be physiologically relevant. The conditional genetic approaches used in this study to manipulate FGFRs specifically in adult astrocytes bypass to a large extent these issues and has allowed us to decipher the direct role of FGF signaling in astrocytes in the injured neocortex. The results prompt a reconsideration of FGFs role in astrocyte function; rather than promote astrocyte activation, FGFs act at different stages of the injury response to directly suppress astrocyte activation.

Other than FGFs, two factors have previously been identified as required in astrocytes to inhibit aspects of activation. Deletion of β-integrin in embryonic astrocytes results in astrocyte activation in postnatal mice, and deletion of *Smoothened*, a mediator of SHH signaling, at early postnatal stages leads to features of astrogliosis in the adult forebrain (8, 9). It remains unclear whether other factors are also required to actively maintain the nonreactive state of cortical astrocytes under normal conditions or to regain their nonreactive state when damage has been contained. Interestingly, similar to the deletion of FGFRs, deletion of *Smoothened* specifically in adult astrocytes also leads to their decreased ability to proliferate after injury (20).

Astrogliosis is also likely to be regulated differently in other parts of the CNS. In our studies, loss of *Fgfr3* alone is not sufficient to cause the activation of astrocytes in the forebrain (Table 1). Unlike in the forebrain of *Fgfr3*-null mice, increased GFAP expression is observed in astrocytes in the spinal cord (39). However, because *Fgfr3* is missing from all cell types from embryogenesis onward, whether the reactive astrocytes observed in the spinal cord of these mutant mice result from an inability of *Fgfr1* and *Fgfr2* to compensate in spinal cord astrocytes compared with forebrain astrocytes or indirectly from developmental or other spinal cord defects remains unclear. Nevertheless, in the present study, loss of *Fgfr3* (conditionally or as a null) combined with loss of one or both of the other receptors is essential for astrocyte activation (Table 1), suggesting that, among the three receptors, FGFR3 carries most of the signaling load.

After damage is removed or contained, surrounding astrocytes typically return to a nonreactive state. The timely resolution of astrogliosis is important for neural tissue to return to homeostasis and for avoiding deleterious consequences. Because few inhibitors of astrocyte activation had been identified and the expression of proinflammatory factors is transient after damage, the resolution of astrocyte activation could have simply been a passive process mediated by the down-regulation of proinflammatory factors. In this study, we found that reducing FGF signaling results in impaired resolution of the injury-induced activation of astrocytes outside the scar, whereas the scar itself is smaller likely because of the inability of astrocytes to proliferate. Conversely, increasing signaling is sufficient to improve resolution, suggesting that, in addition to the down-regulation of proinflammatory factors, suppressors such as FGFs are critical for actively reestablishing the normal nonreactive state of astrocytes after injury. Consistent with these findings, in astrocyte cultures, FGF2 inhibits GFAP expression, TGFβ1 promotes GFAP expression, and, interestingly, FGF2 inhibits the TGFβ1-mediated increase in GFAP (16).

Although they interfere with axonal and cellular regeneration (40, 41), astrogliosis and scar formation are essential for minimizing the spread of damage. Chronic astrogliosis can also interfere with normal brain function (38). Hence, the precise regulation of astrogliosis is critical for optimal neurological function. In sum, we demonstrate that the astrocytic response to injury is not only controlled by a positive feed-forward mechanism but is also normally under negative regulation by FGF and selectively derepressed upon injury. These findings suggest that manipulating FGF signaling in astrocytes could potentially improve functional recovery without compromising tissue integrity in neuropathological conditions.

Materials and Methods

Mice and TM Treatment. The transgenic GOF line, which conditionally expresses a constitutively active FGFR3, was generated as follows. The coding sequence for FGFR3TDII^{K650E} (provided by Jing Chen, Emory University, Atlanta, GA) was placed upstream of an IRES-eGFP (from plasmid 381, provided by Antonello Mallamaci, Scuola Internazionale Superiore di Studi Avanzati, Italy) and these were placed downstream of a lox-stop-lox cassette and the CAG promoter (pCAG-GFP; Addgene). Five founder lines were established by crossing to Swiss–Webster mice and genotyped by using the following primers: 5′-CACGATGATAATATGGCCACAAC; 5′-CGTCCTTGAAGAAGATGGTGC. Mice carrying one copy of the Nestin-CreER allele and one copy of the FGFR3 GOF allele from transgenic founder line 10, which expressed intermediate levels of protein upon recombination, were used for all experiments. The mutant *Fgfr*, *Nestin-CreER*, *Rosa26*$^{lox\text{-}stop\text{-}lox\text{-}EGFP}$ reporter, and *CamK2a-CreER* mice were described previously (17, 18, 42–46). Two- to three-month-old adult mice were used at the start of each experiment. TM was dissolved in corn oil at 20 mg/mL; 5 mg/35g TM was administered intraperitoneally every other day for a total of five doses. Brains were collected for analysis at different time points as indicated in the text.

Immunostaining. Mice were perfused intracardially by using 4% (g/100 mL) paraformaldehyde (PFA) and postfixed overnight in 4% PFA at 4 °C, cryoprotected in 20% sucrose, and embedded in optimum cutting temperature compound. Tissue was cryosectioned at 20 μm. Immunostaining was performed according to standard methods. For immunofluorescence, sections were incubated with primary antibodies in blocking solution overnight at 4 °C, incubated with appropriate Texas Red or FITC-conjugated secondary

antibodies in blocking solution for 1 h at room temperature, and mounted in FluoroMount G. For Ki-67 staining, before blocking in goat serum, sections were heated in 10 mM sodium citrate, pH 6.0, in a microwave oven for antigen retrieval. Immunohistochemical staining for GFAP was performed by using DAB chromogen staining (ABC kit; Vector Laboratories) or immunofluorescence. A cell colabeled for GFAP and Ki-67 is one in which cytoplasmic GFAP staining surrounds most or all of a Ki-67$^+$ nucleus. Orthogonal views are shown for the control in Fig. 7*B* as an example of colabeling. TUNEL staining was performed following the manufacturer's protocol (Roche). All sections for analysis were matched along the anterior–posterior axis.

The following primary antibodies were used: rabbit anti–caspase-3 (1:200; Cell Signaling), mouse anti-NeuN (1:100; Millipore), rabbit anti-Iba1 (1:500; Wako), rabbit anti-GFAP (1:500; Dako Cytomation), mouse anti–Ki-67 (1:100; BD Pharmingen), rat anti-CD45 (1:50; Serotec), rabbit anti-S100 (1:100; Sigma), mouse anti-S100β (1:1,000; Sigma), rabbit anti-GFP (1:100; Invitrogen), rat anti-Nestin (1:100; BD Pharmingen), mouse anti-vimentin (1:2; Hybridoma Bank), rabbit anti-Olig2 (1:400; Millipore), rabbit anti-laminin (1:200; Millipore), rat anti-TenascinC (1:400; Abcam), and rabbit anti-NG2 (1:200; Millipore). Sections were analyzed by conventional fluorescence microscopy (AxioSkop2 p; Zeiss) except for GFAP/Ki-67 colabeling experiments, which were analyzed by confocal fluorescence microscopy (FluoView 500; Olympus).

Astrocyte Volume Measurement. For the uninjured brains, LOF mutants carrying the GFP reporter allele and littermate controls (*NestinCreER*;*Fgfr1*$^{fx/fx}$;*Fgfr2*$^{fx/fx}$;*Fgfr3*$^{-/+}$;*Rosa26*$^{lox\text{-}stop\text{-}lox\text{-}EGFP}$) were used for measuring astrocyte cell volume. Animals were treated with TM as described earlier, and brains were collected and analyzed after 3 wk. Cryosections (20 μm) were subjected to double immunofluorescence staining for GFAP and GFP. *Z*-stacks were taken with a Zeiss LSM 510 Meta Duo V2 confocal microscope with a ×63 objective. Cell volumes were determined by using MetaMorph software. Three separate experiments were performed, and at least five cells were measured for each animal. For the injured brains, LOF mutants, GOF mutants, and controls were stained for GFAP and astrocyte volume measured as described earlier for GFP.

Combined FISH and Immunohistochemistry. The method was adapted from a previously described protocol (47). Briefly, 20-μm cryosections mounted on glass slides were fixed in 4% PFA for 15 min and washed three times with PBS solution. Endogenous peroxidases were inactivated with 2% H_2O_2 for 30 min followed by three 5-min washes in PBS solution. The slides were then incubated with 1 μg/mL protease K in 5 mM EDTA and 50 mM Tris·HCl (pH 7.0) for 20 min. After rinsing in water briefly, the slides were acetylated for 15 min in 0.25% acetic anhydride in 100 mM triethanolamine, pH 8.0, followed by equilibration in 5× SSC and prehybridization in hybridization buffer (50% formamide, 5× SSC, 5× Denhardt, 100 μg/mL yeast RNA, and 10% dextran sulfate) at 65 °C for 2 h. Hybridization was carried out in the same buffer in the presence of the heat-denatured digoxigenin-labeled RNA probes (1:1,000 dilution) for 40 h at 65 °C. After hybridization, slides were washed at 65 °C in wash buffer (1× SSC, 50% formamide, and 0.1% Tween-20) twice for 30 min followed by three 5-min washes in MABT buffer (100 mM maleic acid, 150 mM NaCl, and 0.1% Tween-20, pH 7.5). Slides were then blocked for 1 h in blocking buffer (MABT buffer, 2% Roche blocking reagent, and 10% sheep serum) at room temperature, followed by incubation overnight at 4 °C with anti–digoxigenin-polymerized-peroxidase (Roche) diluted 1:1,000 in blocking buffer. After being washed three times in MABT buffer, slides were incubated with Cy3-tyramide amplification reagent working solution (Perkin-Elmer) for 3–10 min at room temperature followed by three 5-min washes in PBS solution with 0.1% Triton X-100. Immunohistochemistry was then performed as described earlier. A cell was considered positive for *Fgfr1* or *Erm* if more than five bright spots were found in contact or overlapping with the Hoechst 33342 (1 μm/mL)-stained nucleus.

Western Blot Analysis. At week 4 after TM treatment, mouse cortices were dissected and homogenized in ice-cold lysis buffer (25 mM Tris·HCl, pH 7.4, 150 mM NaCl, 5 mM EDTA, pH 8.0, 5 mM EGTA, pH 8.0, 0.5% Triton X-100, 1% phosphatase inhibitor, 1% protease inhibitor). Protein concentrations were measured by using the Pierce BCA protein assay kit. Twenty micrograms of total protein extracts were resolved on 4–12% Bis-Tris acrylamide gels and transferred to nitrocellulose membrane. The following primary antibodies were used: phospho-p44/42 MAPK (pErk1/2; Thr202/Tyr204; 1:1,000; Cell Signaling), p44/42 MAPK (Erk1/2; 1:1,000; Cell Signaling), Phospho-Smad3 (S423/425; 1:1,000; Cell Signaling), Smad2 (1:1,000; Cell Signaling), Phospho-Akt (Ser473; 1:1,000; Cell Signaling), Akt (1:1,000; Cell Signaling), NF-κB p65 (1:400; Santa Cruz), Lhx2 (1:5,000; provided by Elaine Fuchs, Rockefeller University, New York), Cdc42 (1:200; Santa Cruz), and β-tubulin (1:10000; Sigma). Horseradish-conjugated secondary antibodies (1:250; Jackson Immunoresearch) were used. Chemiluminescent signals were detected by using Amersham ECL Plus Western Blotting Detection Reagents.

Ibuprofen and Rapamycin Treatments. Mice were treated with TM as described earlier. For ibuprofen treatment, after the last dose of TM, mice were fed with chow containing ibuprofen (375 ppm; Research Dies) or regular diet as described previously (48, 49) for 3 wk before collecting brains for analysis. For rapamycin treatment, after the last dose of TM, mice received daily 10 mg/kg i.p. injections of rapamycin (50, 51) three times per week for 3 wk before collecting brains for analysis. For both drugs, brains were sectioned and analyzed by immunofluorescence for changes in GFAP staining as described earlier.

Fluro-Jade B Staining. For the detection of degenerating neurons, Fluoro-Jade B staining was performed on sections by using a previously described method (52). Briefly, cryosections were washed with PBS solution and then immersed in 100% ethanol for 3 min followed by a 1-min rinse in 70% ethanol and 1 min in distilled water. The slides were then incubated in 0.06% potassium permanganate for 15 min and rinsed in water before transferring to the 0.001% Fluoro-Jade B solution in 0.1% acetic acid for 30 min. After staining, the slides were rinsed in water and air-dried on a hotplate. The sections were then cleared by immersion in xylene for 10 min and coverslipped with Permount.

Flow Cytometry. Brains from *Nestin-CreER*;*Rosa26*$^{lox\text{-}stop\text{-}lox\text{-}EGFP}$ and *Nestin-CreER*;*Fgfr1*$^{fx/fx}$;*Fgfr2*$^{fx/fx}$;*Fgfr3*$^{-/-}$;*Rosa26*$^{lox\text{-}stop\text{-}lox\text{-}EGFP}$ mice were collected 3–4 wk after TM treatment. Cortices from two or three mice from each genotype were dissected free of white matter, cut into small pieces, and digested with papain solution (0.1% papain/1 mM cysteine HCl/0.5 mM EDTA) for 1 h. The tissue was then triturated in cold DMEM/F12 containing 0.5 mg/mL DNase I and 0.7 mg/mL ovomucoid. The dissociated cells were collected by spinning over a 22% Percoll gradient. GFP$^+$ cells were then sorted by using a Dako Cytomation MoFlo cell sorter flow cytometer. Purified cells were immediately subjected to RNA extraction.

Real-Time PCR. RNA was extracted following manufacturer's protocol (RNeasy Micro Kit; Qiagen). cDNA was synthesized by using the iScript cDNA Synthesis Kit (Bio-Rad). Real-time PCR was carried out in triplicate for each sample with a SYBR Green PCR mixture (Applied Biosystems) with an ABI PRISM 7300 real-time PCR system (Applied Biosystems). Relative RNA levels and statistical comparisons were calculated by using the relative expression software tool (REST) program. Target gene expression was normalized to *Gapdh* expression and shown relative to control samples.

Analysis of the Blood–Brain Barrier. Three weeks after TM treatment, fluorescence tracers were administered intraperitoneally into control and mutant mice, which were killed 1 h later. Brains were collected and fixed overnight at 4 °C in 4% PFA, cryoprotected in 20% sucrose, and embedded in optimum cutting temperature compound. Evans blue solution (200 μL/30 g body weight; 0.5% in PBS solution) and 5 mL/kg of sodium fluorescein (376 Da; 10% solution) were used.

Stab Wound Injury. Cortical stab wounds were carried out as previously described (4) 3 wk after TM treatment. The surgery was performed under a stereotaxic apparatus. Injuries were made through the cortex with a sterile number 11 scalpel blade at 1.5 mm lateral to the midline, 1 mm posterior to bregma and 3.5 mm deep from the skull surface with the stab length in the anterior–posterior axis. One, three, and twenty days after the surgery, brains were perfused with 4% PFA and collected for analysis.

Cell Counts. Cell counting was carried out by using sections that were positionally matched in control and mutant littermates. Statistical analyses were performed by Student *t* test. At least three sections from both hemispheres for each of three independent experiments were used for cell counts. The numbers were averaged and compared between mutant and control littermates.

Quantification of GFAP Staining Intensities After Injury. For the stab wound injury experiments, MetaMorph software was used to measure the intensity of GFAP staining after thresholding to exclude low-intensity pixels (≥100, with a maximum of 255). The integrated GFAP staining intensity was determined in boxed areas (780 × 550, 640 × 410, and 770 × 400 μm for 1, 3, and 20 d post injury, respectively) positioned 100 μm above the top edge of the corpus callosum, immediately outside the lesioned area (except for the 20-d time point, in which case the boxed area was 130 μm from the lesion to avoid the scar), and with the length of the box parallel to the surface of the

neocortex (Fig. 6). The lesion is defined as the GFAP-negative (generally acellular) area of the injury. Values were normalized to those in the same position of the uninjured contralateral hemisphere. For scar tissue measurements, a 650 × 400 μm grid comprised of 13 × 8 squares (50 × 50 μm) was centered on the injury site with the deepest edge of the grid coinciding with the deepest positive square (defined as having a total of all of the pixel intensity values in that square greater or equal to threshold). The integrated intensity and integrated area of GFAP staining were measured for each square in the grid. The total integrated area from all positive squares was used as a measure of the area of a scar. The total integrated intensities from all positive squares were used as a measure for the integrated GFAP staining intensity of a scar (Fig. 7).

LV Transduction in Vivo. Two lentiviral vectors were used. The mutant vector contains the cDNA sequence of a constitutively active FGFR3 mutant, FGFR3 TDII^{K650E} (as detailed earlier) downstream of a ubiquitous CAG promoter and followed by an IRES-eGFP sequence (LV- FGFR3*-GFP). The control vector contains only the eGFP sequence downstream of the CAG promoter (LV-GFP). Concentrated LV (in 1.5 μL) was injected stereotaxically into the neocortex (1.5 mm lateral to the midline, 1.5 mm posterior to bregma, and 1.5 mm deep from the skull surface) of WT adult mice. Brains were collected 2 wk after injection. Images around the injection sites were taken by using a confocal microscope. In each image, the mean GFAP fluorescence intensity was determined in GFP$^+$ and GFP$^-$ cells by using MetaMorph software. The values of the mean GFAP intensity in GFP$^+$ cells versus the mean GFAP intensity in GFP$^-$ cells were compared between the mutant and control animals.

ACKNOWLEDGMENTS. The authors acknowledge the experimental assistance of Rachel Fremont and Kamran Khodakhah (stab wound injury), Adrianna Latuszek (virus), Jee-Yeon Hwang and Susan Zukin (quantitative real-time PCR), Grigoriy Gutin (cell sorting), and Kevin Fisher (software development). This work was supported by National Institutes of Health Grants R21NS073761, R01MH083804, R01MH070596, R01NS039007 (to G.F.), R01NS30989 (to G.F.), R01NS045217 (to G.F.), and R01MH071679 (to G.F.); the Hirschl/Weill-Caulier Foundation; and the Simons Foundation (G.F.).

1. Zhang Y, Barres BA (2010) Astrocyte heterogeneity: An underappreciated topic in neurobiology. *Curr Opin Neurobiol* 20(5):588–594.
2. Sofroniew MV, Vinters HV (2010) Astrocytes: Biology and pathology. *Acta Neuropathol* 119(1):7–35.
3. Kang W, Hébert JM (2011) Signaling pathways in reactive astrocytes, a genetic perspective. *Mol Neurobiol* 43(3):147–154.
4. Bush TG, et al. (1999) Leukocyte infiltration, neuronal degeneration, and neurite outgrowth after ablation of scar-forming, reactive astrocytes in adult transgenic mice. *Neuron* 23(2):297–308.
5. Faulkner JR, et al. (2004) Reactive astrocytes protect tissue and preserve function after spinal cord injury. *J Neurosci* 24(9):2143–2155.
6. Ariel A, Timor O (2013) Hanging in the balance: Endogenous anti-inflammatory mechanisms in tissue repair and fibrosis. *J Pathol* 229(2):250–263.
7. Serhan CN, Chiang N, Van Dyke TE (2008) Resolving inflammation: Dual anti-inflammatory and pro-resolution lipid mediators. *Nat Rev Immunol* 8(5):349–361.
8. Garcia ADR, Petrova R, Eng L, Joyner AL (2010) Sonic hedgehog regulates discrete populations of astrocytes in the adult mouse forebrain. *J Neurosci* 30(41):13597–13608.
9. Robel S, et al. (2009) Conditional deletion of beta1-integrin in astroglia causes partial reactive gliosis. *Glia* 57(15):1630–1647.
10. Ridet JL, Malhotra SK, Privat A, Gage FH (1997) Reactive astrocytes: Cellular and molecular cues to biological function. *Trends Neurosci* 20(12):570–577.
11. Reilly JF, Kumari VG (1996) Alterations in fibroblast growth factor receptor expression following brain injury. *Exp Neurol* 140(2):139–150.
12. Clarke WE, Berry M, Smith C, Kent A, Logan A (2001) Coordination of fibroblast growth factor receptor 1 (FGFR1) and fibroblast growth factor-2 (FGF-2) trafficking to nuclei of reactive astrocytes around cerebral lesions in adult rats. *Mol Cell Neurosci* 17(1):17–30.
13. Eclancher F, Perraud F, Faltin J, Labourdette G, Sensenbrenner M (1990) Reactive astrogliosis after basic fibroblast growth factor (bFGF) injection in injured neonatal rat brain. *Glia* 3(6):502–509.
14. Menon VK, Landerholm TE (1994) Intralesion injection of basic fibroblast growth factor alters glial reactivity to neural trauma. *Exp Neurol* 129(1):142–154.
15. Goddard DR, Berry M, Kirvell SL, Butt AM (2002) Fibroblast growth factor-2 induces astroglial and microglial reactivity in vivo. *J Anat* 200(pt 1):57–67.
16. Reilly JF, Maher PA, Kumari VG (1998) Regulation of astrocyte GFAP expression by TGF-β1 and FGF-2. *Glia* 22(2):202–210.
17. Balordi F, Fishell G (2007) Mosaic removal of hedgehog signaling in the adult SVZ reveals that the residual wild-type stem cells have a limited capacity for self-renewal. *J Neurosci* 27(52):14248–14259.
18. Sousa VH, Miyoshi G, Hjerling-Leffler J, Karayannis T, Fishell G (2009) Characterization of Nkx6-2-derived neocortical interneuron lineages. *Cereb Cortex* 19(suppl 1):i1–i10.
19. Krum JM, Rosenstein JM (1999) Transient coexpression of nestin, GFAP, and vascular endothelial growth factor in mature reactive astroglia following neural grafting or brain wounds. *Exp Neurol* 160(2):348–360.
20. Sirko S, et al. (2013) Reactive glia in the injured brain acquire stem cell properties in response to sonic hedgehog. [corrected]. *Cell Stem Cell* 12(4):426–439.
21. Buffo A, et al. (2005) Expression pattern of the transcription factor Olig2 in response to brain injuries: implications for neuronal repair. *Proc Natl Acad Sci USA* 102(50):18183–18188.
22. Gehrmann J, Matsumoto Y, Kreutzberg GW (1995) Microglia: Intrinsic immuneffector cell of the brain. *Brain Res Brain Res Rev* 20(3):269–287.
23. Perry VH, Andersson PB, Gordon S (1993) Macrophages and inflammation in the central nervous system. *Trends Neurosci* 16(7):268–273.
24. Abbott NJ, Rönnbäck L, Hansson E (2006) Astrocyte-endothelial interactions at the blood-brain barrier. *Nat Rev Neurosci* 7(1):41–53.
25. Oikawa H, Hayashi K, Maesawa C, Masuda T, Sobue K (2010) Expression profiles of nestin in vascular smooth muscle cells in vivo and in vitro. *Exp Cell Res* 316(6):940–950.
26. Benner EJ, et al. (2013) Protective astrogenesis from the SVZ niche after injury is controlled by Notch modulator Thbs4. *Nature* 497(7449):369–373.
27. Barnabé-Heider F, et al. (2010) Origin of new glial cells in intact and injured adult spinal cord. *Cell Stem Cell* 7(4):470–482.
28. Sabelström H, et al. (2013) Resident neural stem cells restrict tissue damage and neuronal loss after spinal cord injury in mice. *Science* 342(6158):637–640.
29. Lacroix S, et al. (2014) Central canal ependymal cells proliferate extensively in response to traumatic spinal cord injury but not demyelinating lesions. *PLoS ONE* 9(1):e85916.
30. Goetz R, Mohammadi M (2013) Exploring mechanisms of FGF signalling through the lens of structural biology. *Nat Rev Mol Cell Biol* 14(3):166–180.
31. Robel S, Bardehle S, Lepier A, Brakebusch C, Götz M (2011) Genetic deletion of cdc42 reveals a crucial role for astrocyte recruitment to the injury site in vitro and in vivo. *J Neurosci* 31(35):12471–12482.
32. de Melo J, et al. (2012) Injury-independent induction of reactive gliosis in retina by loss of function of the LIM homeodomain transcription factor Lhx2. *Proc Natl Acad Sci USA* 109(12):4657–4662.
33. Tavormina PL, et al. (1995) Thanatophoric dysplasia (types I and II) caused by distinct mutations in fibroblast growth factor receptor 3. *Nat Genet* 9(3):321–328.
34. Webster MK, D'Avis PY, Robertson SC, Donoghue DJ (1996) Profound ligand-independent kinase activation of fibroblast growth factor receptor 3 by the activation loop mutation responsible for a lethal skeletal dysplasia, thanatophoric dysplasia type II. *Mol Cell Biol* 16(8):4081–4087.
35. Spassky N, et al. (2005) Adult ependymal cells are postmitotic and are derived from radial glial cells during embryogenesis. *J Neurosci* 25(1):10–18.
36. Mirzadeh Z, Merkle FT, Soriano-Navarro M, Garcia-Verdugo JM, Alvarez-Buylla A (2008) Neural stem cells confer unique pinwheel architecture to the ventricular surface in neurogenic regions of the adult brain. *Cell Stem Cell* 3(3):265–278.
37. Chojnacki AK, Mak GK, Weiss S (2009) Identity crisis for adult periventricular neural stem cells: Subventricular zone astrocytes, ependymal cells or both? *Nat Rev Neurosci* 10(2):153–163.
38. Sofroniew MV (2009) Molecular dissection of reactive astrogliosis and glial scar formation. *Trends Neurosci* 32(12):638–647.
39. Pringle NP, et al. (2003) Fgfr3 expression by astrocytes and their precursors: Evidence that astrocytes and oligodendrocytes originate in distinct neuroepithelial domains. *Development* 130(1):93–102.
40. Pekny M, Nilsson M (2005) Astrocyte activation and reactive gliosis. *Glia* 50(4):427–434.
41. Sofroniew MV (2005) Reactive astrocytes in neural repair and protection. *Neuroscientist* 11(5):400–407.
42. Deng C, Wynshaw-Boris A, Zhou F, Kuo A, Leder P (1996) Fibroblast growth factor receptor 3 is a negative regulator of bone growth. *Cell* 84(6):911–921.
43. Madisen L, et al. (2010) A robust and high-throughput Cre reporting and characterization system for the whole mouse brain. *Nat Neurosci* 13(1):133–140.
44. Trokovic R, et al. (2003) FGFR1 is independently required in both developing mid- and hindbrain for sustained response to isthmic signals. *EMBO J* 22(8):1811–1823.
45. Yu K, et al. (2003) Conditional inactivation of FGF receptor 2 reveals an essential role for FGF signaling in the regulation of osteoblast function and bone growth. *Development* 130(13):3063–3074.
46. Su N, et al. (2010) Generation of Fgfr3 conditional knockout mice. *Int J Biol Sci* 6(4):327–332.
47. Tiveron MC, Hirsch MR, Brunet JF (1996) The expression pattern of the transcription factor Phox2 delineates synaptic pathways of the autonomic nervous system. *J Neurosci* 16(23):7649–7660.
48. Sekiyama K, et al. (2012) Ibuprofen ameliorates protein aggregation and astrocytic gliosis, but not cognitive dysfunction, in a transgenic mouse expressing dementia with Lewy bodies-linked P123H β-synuclein. *Neurosci Lett* 515(1):97–101.
49. Morihara T, et al. (2005) Ibuprofen suppresses interleukin-1beta induction of pro-amyloidogenic alpha1-antichymotrypsin to ameliorate beta-amyloid (Abeta) pathology in Alzheimer's models. *Neuropsychopharmacology* 30(6):1111–1120.
50. Erlich S, Alexandrovich A, Shohami E, Pinkas-Kramarski R (2007) Rapamycin is a neuroprotective treatment for traumatic brain injury. *Neurobiol Dis* 26(1):86–93.
51. Ljungberg MC, Sunnen CN, Lugo JN, Anderson AE, D'Arcangelo G (2009) Rapamycin suppresses seizures and neuronal hypertrophy in a mouse model of cortical dysplasia. *Dis Model Mech* 2(7-8):389–398.
52. Schmued LC, Albertson C, Slikker W, Jr (1997) Fluoro-Jade: A novel fluorochrome for the sensitive and reliable histochemical localization of neuronal degeneration. *Brain Res* 751(1):37–46.